Melting, growth, and faceting of lead precipitates in aluminum

L. Gråbæk* and J. Bohr
Physics Department, Risø National Laboratory, DK-4000 Roskilde, Denmark

H. H. Andersen, A. Johansen, E. Johnson, and L. Sarholt-Kristensen
Physics Laboratory, H. C. Ørsted Institute, Universitetsparken 5, DK-2100 Copenhagen Ø, Denmark

I. K. Robinson
AT&T Bell Laboratories, Murray Hill, New Jersey 07974

(Received 5 February 1991; revised manuscript received 12 August 1991)

Aluminum single crystals cut in the ⟨111⟩ direction were implanted with 2×10^{20} m^{-2} Pb^+ ions at 75 or 150 keV. The implanted insoluble lead precipitated as epitaxially oriented crystallites in the aluminum matrix. The precipitates were studied by x-ray diffraction at Risø, DESY, and Brookhaven National Laboratory, and showed large superheating as well as supercooling during repeated heating cycles. The as-implanted precipitates had a characteristic size of ~140 Å, which grew to 210–260 Å during repeated heating cycles. A detailed annealing study shows that the growth rate of the precipitates changes discontinuously at the onset of melting. This shows that significant precipitate growth takes place by coalescence. The diffracted x-ray intensities showed characteristic truncation rods (streaks), indicating that the solid precipitates were octahedra limited by {111} planes and truncated at the corners by {100} facets.

INTRODUCTION

Aluminum implanted with lead was studied by transmission electron microscopy (TEM) in the late 1960's by Thackery and Nelson.[1] More recently, inclusions in aluminum have been studied by Moore *et al.*[2,3] They found the insoluble lead to precipitate with {111} facets in epitaxial alignment with the aluminum matrix. A renewed surge of interest in epitaxial precipitates, started when vom Felde *et al.*[4] and Templier *et al.*[5] found that solid noble-gas precipitates were growing epitaxially in crystalline solids at temperatures substantially above the triple point for these gases. These studies, together with a number of others, e.g., Refs. 6–8 were all performed with a combination of TEM and electron diffraction on samples with a polycrystalline matrix. A first attempt to use x-ray diffraction with polycrystalline samples was inconclusive.[9] It was, however, realized that if a single-crystal matrix was used, it should be possible to use x-ray diffraction and obtain more quantitative information on the behavior of the precipitates. This was done for samples implanted with rare gas[10,11] and Pb,[11,12] all in an aluminum matrix.

The investigation of small lead particles without a free surface has turned out to be of the utmost importance for the understanding of the process of melting. These studies support the recent observations for crystals with a free surface, which demonstrate the importance of the surface as a nucleation site for the melt. Frenken *et al.*[13,14] and Pluis *et al.*[15,16] have by means of 100-keV proton backscattering found that a quasiliquid layer starts to form at the Pb {110} surface more than 100 K below the bulk melting point. By using a cylindrically cut Pb crystal,[17] a large number of surface orientations could be studied and surface premelting was observed in most cases. Premelting was completely suppressed for the {111} surface and to some extent for the {100} surface. Fuoss, Norton, and Brennan[18] studied premelting of lead surfaces using grazing-angle x-ray diffraction. Yang, Lu, and Wang[19] studied roughening and premelting of a lead (110) surface using high-resolution low-energy electron diffraction (HRLEED). Pokorny and Grimvall observed possible premelting effects in lead from resistance measurements.[20] Surface melting appears to be a relatively general phenomenon seen not only in metallic systems. As an example, the beautiful measurements of melting of thin argon layers on graphite[21,22] may be mentioned. For a recent review on the solid-liquid transition, see Kofman, Cheyssac, and Garrigos.[23]

At each temperature the quasiliquid layer formed on a free surface is in thermodynamic equilibrium with the underlying crystal. The thickness of this layer depends on surface orientation and temperature. Phenomenologically, one can see that surface melting occurs whenever the sum of the specific solid-liquid plus liquid-vapor interface energies is lower than the solid-vapor interface energy. A surface may hence act as a nucleation center for the melt. However, the dependence of the thickness of the quasiliquid layer upon temperature requires a theoretical treatment involving a continuum description.[24,25] Surface melting is generally believed to be the explanation for the fact that superheating of metal crystals with a free surface is virtually never observed, the only example being superheating of small crystallites strictly confined by {111} facets,[26,27] in agreement with the above observation that surface premelting is absent at {111} surfaces.

The observed superheating in these cases is 2–3 K. A nice summary has recently been given by Frenken.[28]

For the present study it is particularly interesting what happens if a free surface is not present. van der Gon *et al.*[29] found that premelting of Pb {110} surfaces could be suppressed by a thin PbO layer. Cheyssac, Kofman, and Garrigos[30] studied lead aggregates in alumina by optical reflectivity measurements where they found a large hysteresis between melting and solidification. In contrast to other experiments, both melting and solidification were here observed at temperatures below the bulk melting point for lead. Size-dependent melting of lead inclusions in silicon monoxide was studied in the electron microscope.[31] Superheating (25 K) of silver crystals covered with gold was found by Daeges, Gleiter, and Perepezko,[32] but alloying between the two metals may have influenced the result. The electron microscopy study of indium precipitates in aluminum by Saka, Nishikawa, and Imura[33] showed superheating as well as supercooling of the precipitates. Also, in a perturbed-angular-correlation (PAC) study of indium inclusions in aluminum, both superheating and supercooling were observed.[34]

Generally, during annealing of inclusions, significant growth is observed. The mechanisms responsible for this growth are still widely discussed. Several growth mechanisms such as loop punching,[35] Ostwald ripening,[36,37] and coalescence of inclusions[36,37] have been suggested. The possible punching of dislocation loops has been widely discussed since it was proposed by Greenwood, Foreman, and Rimmer[35] in 1959. However, for loop punching to take place, a pressure substantially higher than what is normally observed is needed. In the Ostwald ripening process, the larger inclusions grow at the expense of the smaller ones because the probability for capture of inclusion atoms versus the probability of expelling an inclusion atoms favors growth of the larger inclusions. Growth by coalescence of inclusions involves diffusion and collision of inclusions as single objects.

The aim of the present work is to study the melting, solidification, and growth of embedded lead particles in aluminum and to establish the crystallographic orientations of the interfaces. This system is particularly well suited for such studies because of the immiscibility of Pb and Al, where the solubility even in the liquid phase is very small, $\sim 0.2\%$.[38] The experimental techniques were ion implantation and x-ray diffraction.

EXPERIMENT

The aluminum single crystals were 9-mm disks 1–2 mm thick, cut within 1° of the ⟨111⟩ direction. Before implantation the samples were mechanically and electrolytically polished. During implantation, the samples were mechanically scanned behind a 4×1.5-mm^2 slit to obtain a 4-mm-wide implanted strip across the surface. The implantation current was $\sim 30\ \mu$A cm^{-2} behind the slit. This will at most give rise to a temperature increase of a few tens of degrees.[39] Implantations were at 75 or 150 keV to a total fluence of 2×10^{20} Pb$^+$ m^{-2}. Some of the lead was lost through outdiffusion and sputtering during the implantation. The total target available for x-ray-diffraction investigations consisted of $\sim 5\times 10^{19}$ m^{-2} atoms.[39] The concentration within the peak area is ~ 1–2 at. %.

During implantation, the samples were tilted 5° to avoid a strong influence of channeling on the depth distributions. A Monte Carlo simulation using the TRIM computer program[40] gave a mean depth of 300 Å for the 75-keV implantation and 520 Å for the 150-keV implantation. Sputtering during implantation removes approximately 100 Å.

The implanted samples were studied through several annealing sequences (see Table I), in a small transportable vacuum furnace, which could be operated at temperatures in the interval 300–770 K. The design of the furnace allowed x-ray diffraction to be performed at the mentioned temperatures, with free access for the x-rays over a solid angle of 2π.

To study the inclusion growth, an isochronal annealing sequence was carried out on an as-implanted sample. The measuring sequence (sample No. 4) was as follows: The lead (111) peak was scanned at room temperature; then the sample was heated to a preset temperature (without overshooting), kept at that temperature for 90 min, and subsequently cooled to room temperature. Here the lead (111) peak was scanned again. This procedure was repeated for a series of temperatures from room temperature (RT) to 688 K.

X-ray-diffraction measurements were performed at double- and triple-axis spectrometers at the rotating anode at Risø National Laboratory and at the synchrotron radiation laboratory HASYLAB at DESY (Deutsche Elektronen Synchrotron) in Hamburg. Further, a series of measurements were performed with the four-circle diffractometer at beam line X16B at NSLS (the National Synchrotron Light Source) at Brookhaven National Laboratory.

On the double- and triple-axis diffractometers, the diffraction peaks were scanned longitudinally, i.e., along the diffraction vector, and in one or two transverse directions perpendicular to this. Note that if the precipitates are not perfectly aligned with the matrix, this will cause a broadening in the transverse directions only. The flexibility of the four-circle diffractometer at Brookhaven facilitated the search for and study of the truncation rods originating from the facets at the inclusions.

It is of particular interest in this context to be able to judge the total intensity in a given diffraction peak because a decrease of the integrated intensity indicates that melting is in progress. If the resolution is infinitely good and assuming that the intensities in orthogonal directions are mutually independent, then $I_{\rm int}=I_xI_yI_z/H^2$, where I_x, I_y, and I_z are integrated intensities for the three mutually orthogonal directions and H is the peak height. In the case where the out-of-plane resolution is much larger than the width of the Bragg peak, the integrated intensity becomes $I_{\rm int}=I_xI_y/H$. The rotating anode diffractometer is usually operated with the resolution perpendicular to the scattering plane relaxed to $\sim 1°$. To obtain the correct measure for the integrated intensity, one must therefore carefully take into account the ratio between the out-of-plane resolution and the width of the Bragg

peaks, which are of comparable magnitude. Similar considerations are necessary for a detailed account of the in-plane resolution.[41] Fortunately, when the transverse width does not change with temperature, the effect of the out-of-plane resolution becomes unimportant.

The position of the Bragg peaks gives the lattice parameter of the precipitates. Any deviation from tabulated values at ambient pressure may therefore, using appropriate equations of state, provide a measure of the pressure in the inclusions. The width [full width at half maximum (FWHM)] of the Bragg peaks are influenced by the finite size of the crystallites. Hence these widths may be used to estimate the size of the precipitates as described below. As a first approximation, the peak position and FWHM for the Bragg peaks can be determined from fits of Gaussian line shapes to the measured data. To do this properly it is, however, necessary to deconvolute the instrumental resolution from the experimental data. Finally, plane surfaces at the diffracting medium—the precipitates—will give rise to so-called truncation rods or streaks of diffracted intensity in directions perpendicular to the surfaces. Faceting of the pre-

TABLE I. Summary of implantation data, heating sequences, and measurements on lead-implanted aluminum single crystals. The names in the "Place" column refer to the following instruments: Risø, the rotating anode two-axis x-ray diffractometer at Risø; D4 and W1, diffractometers in HASYLAB at DESY, Hamburg; and X16B, a four-circle diffractometer at the National Synchrotron Light Source at Brookhaven National Laboratory.

No.	Sample	Sequence	Temperature range (K)	Measurements	Place
1	2×10^{20} m^{-2}	a	299–678	Pb(111): x, y and rocking scans	Risø
	75 keV	b	678–299	no measurements above 299 K	Risø
2	2×10^{20} m^{-2}	a	299–688	Pb (111); x, y, and rocking scans	Risø
	150 keV	b	688–299	no measurements	Risø
		c	299–678	Pb(111): x, y, and rocking scans	Risø
		d	678–299	no measurements	Risø
		e	300–683	Pb(111): x, y, and rocking scans	W1
		f	683–300	no measurements	W1
		g	300–644	Pb(111): x, y, and circular scans around the (111) peak	W1
		h	644–300	no measurements	W1
3	2×10^{20} m^{-2}	a	300–678	Pb(111): x, y, and z scans	Risø
	150 keV	b	678–301	Pb(111): x, y, and z scans	Risø
		c	301–633	Pb(111): x, y, z, and circular scans around the (111) peak	Risø
		d	633–297	no measurements	Risø
		e	297–663	Pb(111)+Pb(222): x, y, z, and circular scans around the (111) peak	Risø
		f	663–300	Pb(111)+Pb(222): x, y, z, and grid scans around the (111) peak	Risø
		g	300–588	588 K reached from above; scans to check the stability of the molten state	Risø
		h	588–300	no measurements	Risø
		i	300	search for (111) truncation rods at the Al(111) peak	D4
		j	303–663	Pb(111): x, y, and z scans, and scans at (111) and (100) truncation rods	X16B
		k	663–303	no measurements	
		l	303–662	Pb(111); x, y, and z scans, and scans at (111) and (100) truncation rods	X16B
		m	662–303	Pb(111): x scans, and scans at (111) and (100) truncation rods	X16B
4	2×10^{20} m^{-2}	a	300–688	Pb(111): x scans;	Risø
	150 keV			isochronal annealing sequence, (see the text)	

cipitates may hence be judged from the existence of such truncation rods.

RESULTS AND DISCUSSION

The nature of the diffraction data obtained is shown in Fig. 1. A clearly resolved Pb(111) peak rising more than two orders of magnitude above the background is observed. Even though the peak is four orders of magnitude below the Al(111) reflection, not only may the peak position be precisely determined, but a detailed shape analysis can also be accomplished. Analysis of the peak position both in the as-implanted state and after the annealing cycles gave lattice parameters in agreement with tabulated bulk values (see Fig. 2). There is hence no evidence for the lead being under a high pressure, as has otherwise been observed for noble-gas precipitates.[10,11] From the uncertainty of the lattice parameter determinations and the known compressibility of lead, an upper limit for the pressure is determined to be 0.18 GPa.[12] It should, however, be emphasized that this is a conservative upper bound; there is no evidence that the pressure is in fact so high. If the inclusions were in equilibrium with the surface tension, the pressure is expected to be as low as 0.05 GPa.[11] The conservative upper bound on the pressure, 0.18 GPa, corresponds to a maximum of 14-K increase in the melting temperature as estimated from the Clausius-Clapeyron equation[42] $dP/dT=L/T\Delta V$, where p is the pressure, T is the absolute temperature, $L=4.81$ kJ/mol is the latent heat of fusion, and $\Delta V=0.035$ is the relative volume change.[38] As this is significantly smaller than the superheating to be discussed below, it cannot account for the observed effect.

The shape of a diffraction peak from one inclusion is ideally a shape transform of the inclusion convoluted with the instrument resolution. The peak shape obtained here is also affected by the size distribution of the inclusions, and so it should be considered as a sum of the different contributions. Ideally, it should be possible to extract information about size distribution and inclusion shape through a careful analysis of the diffraction peaks. In the following we will consider models where all the in-

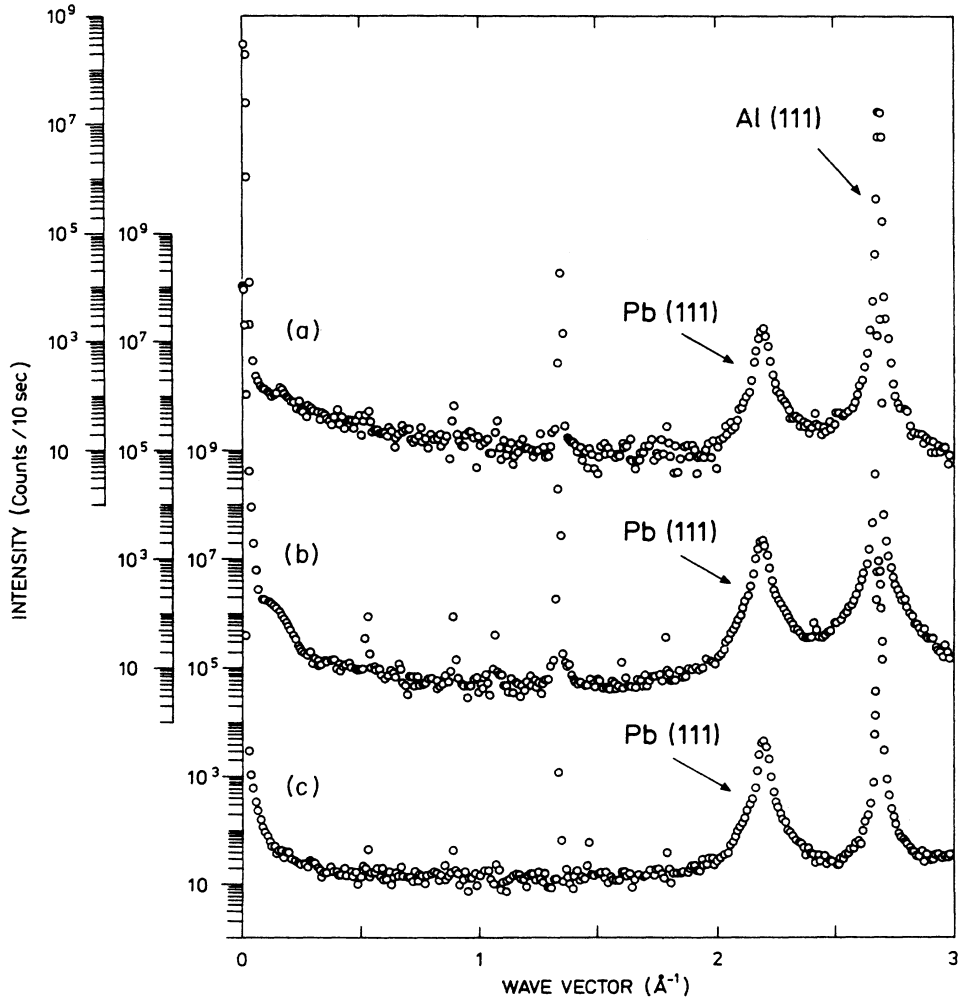

FIG. 1. Longitudinal scans from the *as*-implanted samples Pb-1, Pb-2, and Pb-3 (see Table I). Narrow peaks at smaller wave vectors than the (111) lead peak are higher order reflections from the aluminum matrix.

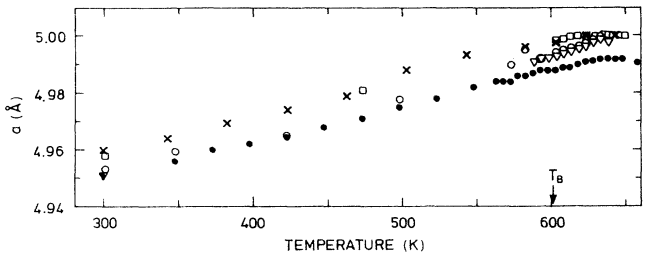

FIG. 2. Lattice constant for the lead in the inclusions as a function of temperature. The lattice constant is determined from the position of the lead (111) peak: cycle 3a (●), cycle 3c (○), cycle 3e (▽), cycle 3j (×), and cycle 3l (□). The arrow marks the bulk melting point T_B.

clusions have the same lattice parameter, resulting in symmetrical diffraction peaks.

The diffraction peak from a nearly monodisperse distribution of inclusions is to a good approximation described by a Gaussian $G(L,q)=\exp[-c(q-q_0)^2/L^2]$, where q is the momentum transfer, q_0 is the position of the diffraction peak, and $c=4(5.57)^2\ln 2$. The inclusion size determined from the full width at half maximum (w_G) for the diffraction peak is $L=5.57/w_G$. The constant 5.57 is determined from the condition that the FWHM of the Gaussian should equal the FWHM of the calculated peak from an inclusion of size L. An example of a fit to one Gaussian is shown in Fig. 3(a) (Pb-3, cycle 3i); the average size obtained from this fit is $L=233$ Å and $\chi^2=2.089$.

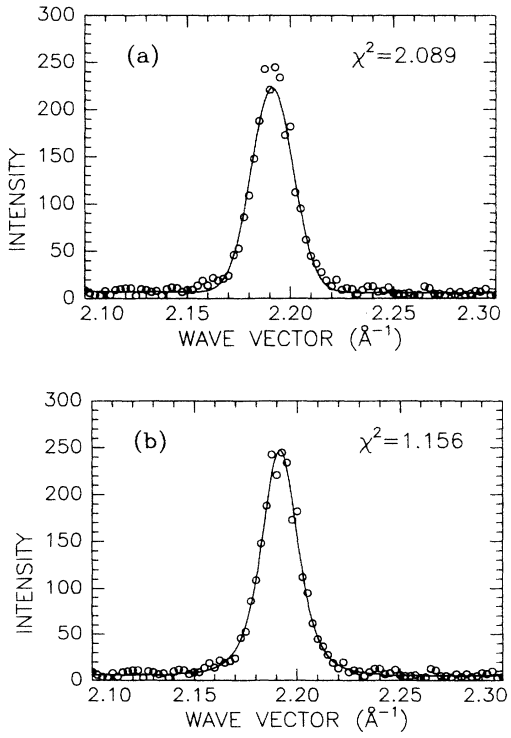

FIG. 3. (111) peak from sample Pb-3, cycle i. The curve in (a) is the best fit using a single Gaussian. From this fit the average size L is determined to be 233 Å. The curve in (b) is the best fit, using the expression (1). From this fit we obtain $\langle L\rangle_v=106$ Å and $w_v=276$ Å. The intensity is expressed in units of counts/4 sec.

The above considerations assumed a monodisperse size distribution. However, in general, the size distribution is not monodisperse.[2,43,44] Let us assume that the distribution of inclusion sizes is such that the probability for an atom to belong to an inclusion of size L can be described by a Gaussian distribution $P_v(L)$, the relative volume fraction. The frequency size distribution is $P_s(L)=P_v(L)/L^3$. For a three-dimensional model, the diffracted intensity can be approximated by the function $L^6G(L,q)$. However, in a diffraction experiment the resolution is not infinitely good. For example, if all out-of-plane intensity is integrated as a result of poor resolution, the power of L is reduced by 1. At D4 (see Table I) a very high resolution was obtained because of the well-collimated beam from the synchrotron and the use of Si monochromator and analyzer crystals. We therefore expect the power of L to be close to 6 for this data set. The complete diffraction peak is hence determined from the integral

$$I(q)=\int_{L_0}^{\infty}L^6G(L,q)P_s(L)dL\ , \tag{1}$$

where

$$P_s(L)=\frac{1}{L^3}P_v(L)$$
$$=\frac{1}{L^3}\exp\left[-4\ln 2\frac{(L-\langle L\rangle_v)^2}{w_v^2}\right], \tag{2}$$

where $\langle L\rangle_v$ is the mean value for $P_v(L)$ and w_v is a width parameter. The lower limit L_0 was chosen to be 55 Å, corresponding to the half width of the scan. The reason for this particular choice is that diffraction peaks from inclusions smaller than 55 Å are so broad that the scattering cannot be distinguished from the background. Nevertheless, the result of the fitting was not very sensitive to the choice of L_0 as long as it was between 0 and 100 Å. Figure 3(b) shows the fit of Eq. (1) to the data in Fig. 3(a). The parameters were $\langle L\rangle_v=106$ Å and $w_v=276$ Å; χ^2 was 1.156. The width of the relative volume fraction is surprisingly large when one considers that the fit to a single Gaussian was almost as good. In conclusion, it is therefore difficult make a quantitative estimate of the width of the size distribution. We also note that a Gaussian line shape is a poor description of the wings of the Bragg peak.

The widths of the diffraction peaks will also be influenced by strain in the inclusions. This may be investigated using the widths of both the (111) and (222) peaks, and the strain is found to be as low as 0.3%,[41] in an annealed sample (Table I). Such a low value is not surprising, considering that a possible overpressure is low and close to being hydrostatic.

Figure 4 shows the longitudinal width for sample No. 4, as the isochronal annealing sequence progresses. As the size of the inclusions is inversely proportional to the

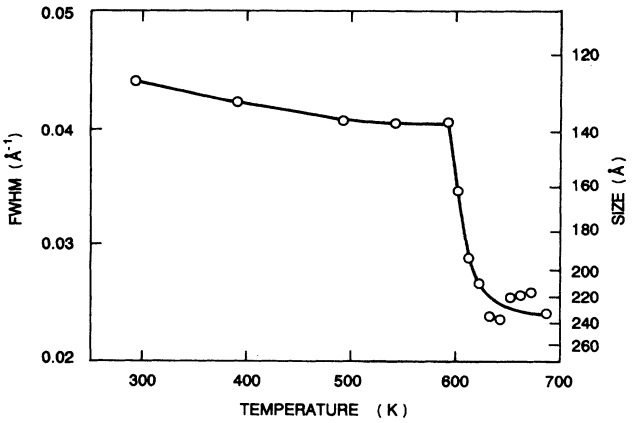

FIG. 4. Full-width at half maximum at room temperature for the (111) lead peak during the isochronal annealing sequence (sample Pb-4), as a function of annealing temperature. The line is only a guide to the eye.

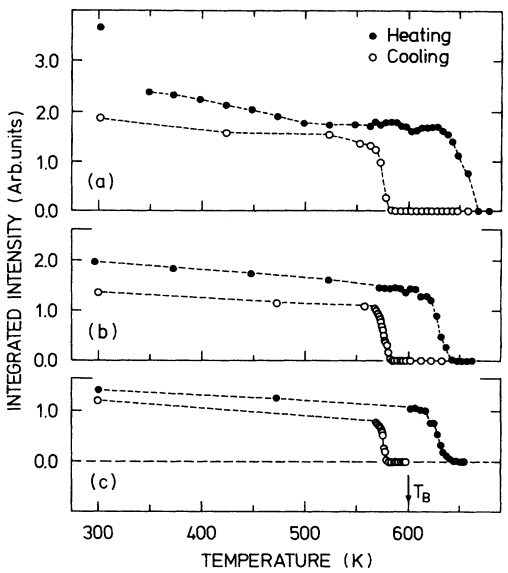

FIG. 5. Integrated intensity for sample Pb-3, heating cycle (a) 3a-b, (b) 3e-f, and (c) 3l-m. The solid circles show data obtained during heating, and the open circles show data obtained during cooling. The arrow marks the bulk melting point T_B.

width, it is seen that the growth rate increases dramatically with temperature. The kink at ~600 K shows a strong discontinuity in the growth rate at this temperature. This demonstrates that the enhanced growth is not due to a simple thermal activation factor. Instead, the enhanced growth must be associated with a phase transformation taking place in the precipitates. The integrated intensity at the annealing temperature starts to decrease at the temperature where a dramatic increase in growth rate is observed. This seems to indicate that the mobility of a fraction of the lead inclusions passes a threshold, allowing them to move and coalesce. We take the observed discontinuity in the mobility of the precipitates as strong evidence for precipitate growth by coalescence of the inclusions and that the discontinuity in the mobility is associated with the onset of melting of the precipitates.

A considerable superheating and supercooling is seen for the lead in the precipitates (see Fig. 5), of which parts (a) and (b) have previously been published in Ref. 12. It is seen that the hysteresis persists through several (in fact, six; see Table I) heating cycles and must hence be considered an intrinsic phenomenon for the inclusions. Further, approximately half a year passed between the data taken for parts (b) and (c). The superheating from the first run (also seen on sample Pb-2) was somewhat higher than during the following heating cycles. We ascribe this to the growth of the inclusions during the first heating cycle as discussed above. Generally, the superheating of ~230 Å inclusions was of the order of 50 K and the supercooling of the order of 20 K. The results obtained for superheating and supercooling of lead in aluminum are in good qualitative agreement with the TEM work on indium inclusions by Saka, Nishikawa, and Imura.[33]

As is seen from Fig. 5 and also described in the text above, we observe a decrease of the superheating from the first to the following heating cycles. Allen, Gile, and Jesser[45] have related the size of a particle to its expected superheating through the relation

$$\frac{T_r}{T_B}=1-\frac{3}{rQ}\left[\frac{\gamma_{SM}}{\rho_S}-\frac{\gamma_{LM}}{\rho_L}\right]+\frac{\Delta E}{Q}\ , \tag{3}$$

where T_r and T_B are the melting temperatures for particles of radius r and for bulk material, respectively. γ_{SM} and γ_{LM} are the specific energies between solid and matrix and liquid and matrix. ρ_S and ρ_L are the densities of solid and liquid lead, respectively, Q the latent heat of melting, and ΔE is the change in strain energy which may come from the physical tendency for lead to expand at melting. As has been demonstrated in the discussion of the pressure in the inclusions, the Clausius-Clapeyron equation shows that ΔE cannot be a dominant term. Further, it is not clear whether the ΔE term plays a role after the sample has been annealed at high temperature.

If the γ's and ρ's are taken to be independent of temperature over the temperature interval where melting takes place, we may write Eq. (3) as

$$T_r=T_B+C_1+\frac{C_2}{r}\ , \tag{4}$$

where C_1 and C_2 are constants. To test this model data pairs (T_r,r) are needed. However, to obtain such data pairs is not trivial. Inclusions of size S_1 are solid at T_1 and melted at T_2, the next higher temperature. We therefore take T_2 to be the melting temperature for inclusions of size S_1, etc. Data obtained according to this prescription are depicted in Fig. 6 together with a fit to the above expression. The resulting constants are $C_1=3$ K and $C_2=2470$ Å K. Considering the difficulties in ascribing pairs of (T_r,r), the value of C_2 is very uncertain and the value of C_1 is somewhat uncertain. The significance of the small value of C_1 is therefore not the value itself, but rather the remarkable agreement between

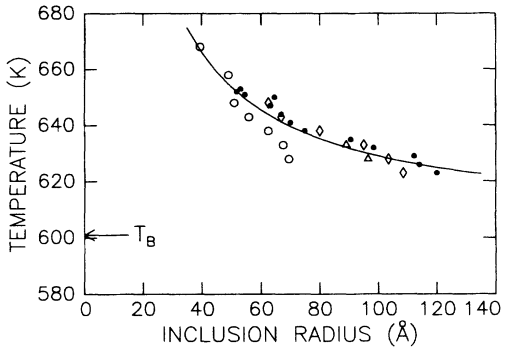

FIG. 6. Melting temperatures as defined in the text for particles of radius r: cycle 3a (○), cycle 3c (△), cycle 3e (◇), and cycle 3l (●). The solid line is the best fit to the expression (4), yielding $C_1=3$ K. The arrow marks the bulk melting point T_B.

the asymptotical value of T_r and the bulk melting point for lead (601 K). In conclusion, the fit clearly shows that the superheating asymptotically disappears with size and that the experimental data are in good agreement with a $1/r$ law.[46] We hence assume that the superheated inclusions are in a stable state. However, we note that homogeneous nucleation of the liquid in the superheated state would also lead to a $1/r$ dependence, implying that the superheated state would be metastable.

The existence of large supercooling makes its plausible that the nucleation of the solid phase appears within the inclusion rather than on the inclusion-matrix interface. Within this framework one can explain the supercooled state of lead as a metastable phase caused by the finite size of the inclusions. Fluid particles (inclusions) smaller than the critical size for homogeneous nucleation of the solid simply appear to be stable, i.e., supercooled.[12] The change in the free energy $\Delta F(d)$ from the appearance of a solid grain of size d in a ΔT supercooled liquid is

$$\Delta F(d)=-\frac{4\pi}{3}\left[\frac{d}{2}\right]^3\frac{L\Delta T}{T_B}+4\pi\left[\frac{d}{2}\right]^2\gamma_{SL}\ , \tag{5}$$

where γ_{SL} is the interface tension between solid and liquid lead, $\gamma_{SL}=33.3$ mJ/m^2.[47] The first term in ΔF is the lowering of the energy from the phase transformation to the solid phase, while the second term is the cost of the additional solid-liquid (SL) interface in the system. As depicted in Fig. 7, the critical size for nucleation, d_c, is determined by differentiation of $\Delta F(d)$ and is $d_c=4\gamma_{SL}T_B/L\Delta T$.[47] Naturally, homogeneous nucleation in this sense cannot take place if the critical size for nucleation exceeds the size of the inclusion. This explains the stability of the supercooled phase. One sees that if an inclusion size of 230 Å is taken as the critical size for nucleation, then the necessary supercooling is 13 K. This is less than the observed supercoolings and therefore consistent with the scenario of homogeneous nucleation.

The expression for the critical size for nucleation is derived for an infinitely large system. For an inclusion of finite size d_i, one must also take into account the energy

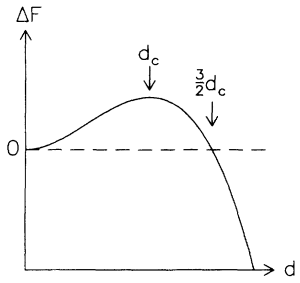

FIG. 7. Excess free energy ΔF for a solid grain of size d in a supercooled liquid. The critical size for nucleation d_c is the minimum size of a grain that would continue to grow in size.

of the interface with the host matrix, i.e., $A(\gamma_{SM}-\gamma_{LM})$, where A is the total interface area between the inclusion and the host matrix, γ_{SM} and γ_{LM} are the interface tensions between solid lead and the aluminum matrix, and liquid lead and the aluminum matrix, respectively. Thus it is not a sufficient condition that $\partial\Delta F/\partial d<0$; rather, for the inclusion to have solidified completely, the condition is

$$-\frac{4\pi}{3}\left[\frac{d_i}{2}\right]^3\frac{L\Delta T}{T_B}+4\pi\left[\frac{d_i}{2}\right]^2(\gamma_{SM}-\gamma_{LM})<0\ . \tag{6}$$

One therefore see that a large value of $\gamma_{SM}-\gamma_{LM}$ would lead to a large supercooling. If the observations of large superheatings is taken as evidence that surface melting (interfacial melting) is preempted, then the inequality $\gamma_{SL}+\gamma_{LM}>\gamma_{SM}$ must hold. From this one can infer that $\gamma_{SM}-\gamma_{LM}<\gamma_{SL}$. The observations of large supercoolings indicate that surface freezing is preempted, i.e., that $(\gamma_{SL}+\gamma_{SM}>\gamma_{LM})$, which leads to the inequality $\gamma_{SM}-\gamma_{LM}>-\gamma_{SL}$. Summarized, one has

$$\gamma_{SL}>\gamma_{SM}-\gamma_{LM}>-\gamma_{SL}\ . \tag{7}$$

Interestingly, the agreement between the critical size for nucleation and inclusion size becomes much better if one takes $\frac{3}{2}d_c$ instead of d_c. This corresponds to the special case where interface energies between the solid (S), liquid

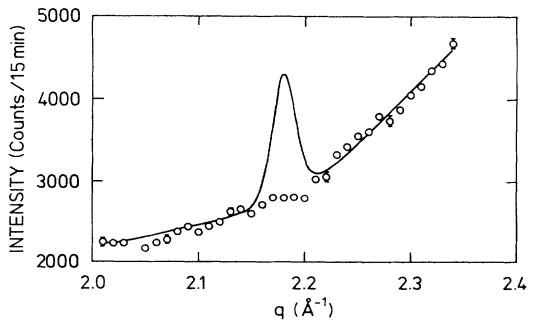

FIG. 8. Longitudinal scan (○) across the expected position of the diffraction sphere from a polycrystalline sample, measured 5° away from the (111) Bragg peak. The solid curve shows the expected peak height provided all the inclusions were solid at the measuring temperature (588 K) but randomly oriented.

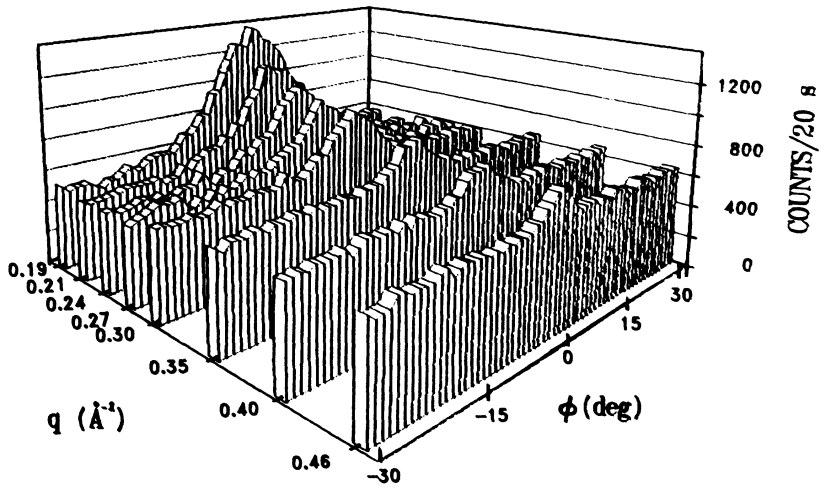

FIG. 9. Three-dimensional plot of the truncation rod originating from the {111} facets at the lead inclusions. Data are obtained at 303 K in cycle 3j and are based on eight scans across the $[\bar{1}\,\bar{1}1]$ truncation rod away from the lead (111) Bragg peak. The distance from the lead peak is given by q, while ϕ gives the distance from the $[\bar{1}\,\bar{1}1]$ direction.

(L), and/or matrix (M) obey the equation $\gamma_{SM}-\gamma_{LM} \simeq \gamma_{LS}$ [see Fig. 7 and compare Eqs. (5)–(7)]. Physically, this may reflect an incoherent interface.

It could be imagined that the inclusions solidify randomly oriented at T_B and that epitaxial alignment is taken up at a lower temperature. If this were the case, the diffraction from the inclusions would appear as a spherical intensity distribution. Several scans across the position where the sphere corresponding to the (111) peak would be seen were performed. Figure 8 shows the negative result of such a search; the solid line shows the expected intensity if the inclusions were solid and randomly oriented. No evidence for such a sphere is found, and it may be concluded that the precipitates at this temperature are indeed liquid. Note that the much broader diffuse sphere from liquid inclusions will not appear at this position as the (111) reflection does not correspond to a nearest-neighbor distance.

The diffracted intensity depicted in Fig. 9 very clearly shows the existence of truncation rods from {111} facets. The figure shows a three-dimensional plot of data obtained at 303 K in cycle 3j. Extensive measurements of these rods were carried out as indicated in Table I. The rod corresponding to the facets of the inclusions parallel to the surface could not be investigated as this rod is completely dominated by intensity from the surface truncation rod of the aluminum crystal. Instead, the truncation rod in the $[\bar{1}\,\bar{1}1]$ direction was analyzed. A similar rod approximately a factor 2.6 weaker was seen in the [100] direction. This is consistent with an inclusion having the shape of an octahedron limited by {111} planes and truncated at the corners by {100} planes. This is in agreement with the earlier TEM observations by Thackery and Nelson[1] and Moore *et al.*[2,3]

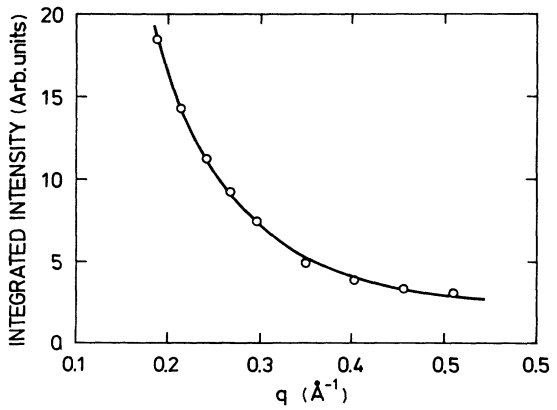

FIG. 10. Integrated intensity of scans across the [111] truncation rod from the lead inclusions, measured along the $[\bar{1}\,\bar{1}1]$ direction. The solid line represents a fit to the expression (8).

The intensity of the truncation rod shown in Fig. 9 can be analyzed to obtain information about the roughness of the facets at the lead crystallites. The integrated intensity is described by Robinson:[48]

$$N_1^2 N_2^2 \frac{(1-\beta)^2}{(1+\beta^2-2\beta\cos qa)} \frac{1}{4\sin^2 \frac{1}{2} qa} . \tag{8}$$

Here N_1 and N_2 represent the scattering components from directions parallel to the facet. The remaining part is due to the component perpendicular to the facet, the component being perturbed by the very existence of the facet. The distance to the lead (111) Bragg peak is given by q; a is the lattice parameter. β is a roughness parameter describing the sharpness of the facet, such that the fractional occupancy of the first noncomplete layer is β and the second is β^2 and so on. The result of fitting this equation to the experimental data is shown in Fig. 10. The roughness parameter β was determined to be 0.13 ± 0.02, which means that the fractional occupancy in the second layer is 0.016, and so the facets of the precipitates are very sharp.

In the cycles 3j and 3l, the rods were studied as a function of temperature. At a number of temperatures, scans

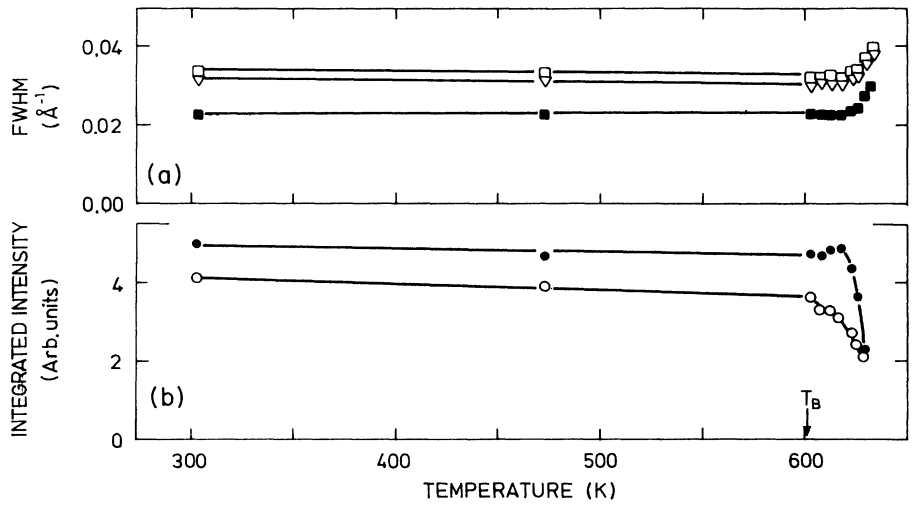

FIG. 11. Upper section: FWHM for the lead (111) peak during annealing cycle 3l: longitudinal x direction (■), transverse y direction (□), and transverse z direction (▽). Lower section: Integrated intensity across the $[\bar{1}\,\bar{1}1]$ rod (●) and the [100] rod (○). The distances to the lead (111) Bragg peak were 0.242 and 0.171 $Å^{-1}$, respectively. The arrow marks the bulk melting point. The integrated intensity for the $[\bar{1}\,\bar{1}1]$ rod starts to decrease around 620 K, the temperature where melting of the lead inclusions start and the width of the Bragg peak starts to increase. The integrated intensity of the [100] rod starts to decrease around 605 K.

were made across the $[\bar{1}\,\bar{1}1]$ and [100] rods at fixed distances from the lead (111) peak. Figure 11 shows the integrated intensities across the rods together with the widths of the (111) Bragg peak. The integrated intensity of the (100) rod starts to decrease around 605 K, while the intensity in the (111) rod starts to decrease around 620 K. This is also the temperature where the integrated intensity for the Bragg peak starts to decrease (Fig. 5). Further, at this temperature the width of the Bragg peak starts to increase (Fig. 10). The different behavior of the (100) rod indicates that premelting or roughening of the {100} facets starts below the temperature where the precipitates in general begin to melt.

CONCLUSIONS

X-ray diffraction has been established as a powerful technique for investigation of epitaxially growing precipitates of nonsoluble implants in crystals. For the particular case of lead in aluminum, the lattice parameter, size, and shape of the crystalline inclusions could be measured.

Large superheating and supercooling of the inclusions were found during melting-solidification cycles. Particularly, the observation of large superheating reveals important information for understanding of the general mechanism of melting for systems without a free surface.

A detailed study of truncation rods originating from the facets showed a difference in behavior at the {100} and {111} facets, indicating that either premelting or roughening of the {100} facets takes place around 605 K, which is ~15 K below the temperature where the inclusions as a whole start to melt. The observed discontinuity in the growth rate for the inclusions demonstrate that melted inclusions grow by migration and coalescence.

ACKNOWLEDGMENTS

We are grateful to J. F. van der Veen for a pertinent discussion and to NSLS, Brookhaven and HASYLAB, DESY for the hospitality we received at these institutions. One of us (L.G.) is grateful to Konsul Axel Nielsens Mindelegat for a grant. This work was in part supported by the Danish Natural Science Research Council.

*Present address: Haldor Topsøe A/S, Nymøllevej 55, 2800 Lyngby, Denmark.

[1]P. A. Thackery and R. S. Nelson, Philos. Mag. **19**, 169 (1969).
[2]K. I. Moore, K. Chattopadhyay, and B. Cantor, Proc. R. Soc. London A **414**, 499 (1987).
[3]K. I. Moore, D. L. Zhang, and B. Cantor, Acta. Metall. **38**, 1327 (1990).
[4]A. vom Felde, J. Fink, Th. Müller-Heinzerling, J. Pfüger, B. Scheerer, G. Linker, and D. Kaletta, Phys. Rev. Lett. **53**, 922 (1984).
[5]C. Templier, C. Jaouen, J. P. Riviere, J. Delafond, and J. Grilhe, C. R. Acad. Sci. Ser. 2 **299**, 613 (1984).
[6]C. Templier, H. Garem, and J. P. Riviere, Philos. Mag. A **53**, 667 (1986).
[7]J. H. Evans and D. J. Mazey, J. Phys. F **15**, 67 (1985).
[8]R. J. Cox, P. J. Goodhew, and J. H. Evans, Acta. Metall. **35**, 2497 (1987).
[9]R. Khanna, A. K. Tyagi, R. V. Nandekar, and G. V. N. Rao, Scr. Metall. **20**, 181 (1986).
[10]H. H. Andersen, J. Bohr, A. Johansen, E. Johnson, L. Sarholt-Kristensen, and V. Surganov, Phys. Rev. Lett. **59**, 1589 (1987).
[11]L. Gråbæk, J. Bohr, E. Johnson, H. H. Andersen, A. Johansen, and L. Sarholt-Kristensen, Mater. Sci. Eng. A **115**, 97

(1989).
[12]L. Gråbæk, J. Bohr, E. Johnson, A. Johansen, L. Sarholt-Kristensen, and H. H. Andersen, Phys. Rev. Lett. **64**, 934 (1990).
[13]J. W. M. Frenken and J. F. van der Veen, Phys. Rev. Lett. **54**, 134 (1985).
[14]J. W. M. Frenken, P. M. J. Marée, and J. F. van der Veen, Phys. Rev. B **34**, 7506 (1986).
[15]B. Pluis, A. W. Renier van der Gon, J. W. M. Frenken, and J. F. van der Veen, Phys. Rev. Lett. **59**, 2678 (1987).
[16]B. Pluis, T. N. Taylor, D. Frenkel, and J. F. van der Veen, Phys. Rev. B **40**, 1353 (1989).
[17]B. Pluis, J. W. M. Frenken, and J. F. van der Veen, Phys. Scr. T **19**, 382 (1987).
[18]P. H. Fuoss, L. J. Norton, and S. Brennan, Phys. Rev. Lett. **60**, 2046 (1988).
[19]H.-N. Yang, T.-M. Lu, and G.-C. Wang, Phys. Rev. Lett. **63**, 1621 (1989).
[20]M. Pokorny and G. Grimvall, J. Phys. F **14**, 931 (1984).
[21]D.-M. Zhu and J. G. Dash, Phys. Rev. Lett. **57**, 2959 (1986).
[22]D.-M. Zhu and J. G. Dash, Phys. Rev. Lett. **60**, 432 (1988).
[23]R. Kofman, P. Cheyssac, and R. Garrigos, Phase Transitions, **B24-26**, 283 (1990).
[24]R. Lipowsky, Phys. Rev. Lett. **49**, 1575 (1982).
[25]R. Lipowsky and W. Speth, Phys. Rev. B **28**, 3983 (1983).
[26]G. D. T. Spiller, Philos. Mag. A **46**, 535 (1982).
[27]J. J. Métois and J. C. Heyraud, J. Phys. (Paris) **50**, 3175 (1989).
[28]J. W. M. Frenken, Endeavour **14**, 2 (1990).
[29]D. van der Gon, A. W. Pluis, B. Smith, and J. F. van der Veen, Surf. Sci. **209**, 431 (1989).
[30]P. Cheyssac, R. Kofman, and R. Garrigos, Phys. Scr. **38**, 164 (1988).
[31]Y. Lerah, G. Deutcher, P. Cheyssac, and R. Kofman, Europhys. Lett. **12**, 709 (1990).
[32]J. Daeges, H. Gleiter, and J. H. Perepezko, Phys. Lett. A **119**, 79 (1986).
[33]H. Saka, N. Niskikawa, and T. Imura, Philos. Mag. A **57**, 895 (1988).
[34]G. J. Kemerink, F. Pleiter, and G. H. Kruithof, Hyperfine Interact. **35**, 619 (1987).
[35]G. W. Greenwood, A. J. E. Foreman, and D. E. Rimmer, J. Nucl. Mater. **1**, 305 (1959).
[36]J. Rothaut, H. Schroeder, and H. Ullmaier, Philos. Mag. A **47**, 781 (1983).
[37]H. Trinkaus, Scr. Metall. **23**, 1773 (1989).
[38]*Smithells Metals Reference Book,* edited by E. A. Brandes (Butterworths, London, 1983).
[39]E. Johnson, L. Gråbæk, J. Bohr, A. Johansen, L. Sarholt-Kristensen, and H. H. Andersen, in *Beam-Solid Interactions: Physical Phenomena,* edited by J. A. Knapp, P. Børgesen, and R. A. Zuhr, MRS Symposia Proceedings 157 (Materials Research Society, Pittsburgh, 1990), pp. 247–252.
[40]J. P. Biersack and L. G. Haggmark, Nucl. Instrum. Methods **174**, 257 (1980).
[41]L. Gråbæk, Ph. D. thesis, Roskilde, Denmark, 1990.
[42]L. D. Landau and E. M. Lifshitz, *Course on Theoretical Physics: Statistical Physics* (Pergamon, Oxford, 1980), Vol. 5, Pt. 1, pp. 255–256.
[43]R. C. Birtcher and A. S. Liu, J. Nucl. Mater. **165**, 101 (1989).
[44]K. Tsumuraya and Y. Miyata, Acta. Metall. **31**, 437 (1983).
[45]G. L. Allen, W. W. Gile, and W. A. Jesser, Acta. Metall. **28**, 1695 (1980).
[46]We note that the other powers of r or an exponential can also be fitted to the data, but there is no obvious physical basis for such a description.
[47]D. A. Porter and K. E. Easterling, *Phase Transformations in Metals and Alloys* (Van Nostrand Reinhold, Wokingham, U.K., 1981), pp. 171 and 186–198.
[48]I. K. Robinson, Phys. Rev. B **33**, 3830 (1986).